Progress In Electromagnetics Research, Vol. 135, 641–656, 2013

ROTATIONALLY SYMMETRIC COUPLED-LINES BANDPASS FILTER WITH TWO TRANSMISSION ZEROS

Sai Wai Wong[1, *], Kai Wang[1], Zhining Chen[2, 3], and Qingxin Chu[1]

[1]School of Electronic and Information Engineering, South China University of Technology, Guangzhou, China

[2]The Institute for Infocomm Research, Singapore

[3]Department of Electrical and Computer Engineering, National University of Singapore, Singapore

Abstract—A rotationally symmetric short-circuited stub-loaded structure is proposed to design a microstrip-line bandpass filter with two transmission zeros near the lower and upper cut-off frequency edges of operating millimeter-wave bands. Furthermore, interdigital coupled-lines and additional resonators are integrated into the proposed rotationally symmetric bandpass filter to improve the out-of-band rejection. As design examples, the in-band and out-of-band performances of two filter prototypes using single layer microstrip-lines are designed and experimentally examined. The measured results show that the filter without any interdigital coupled-lines achieves a passband insertion loss of 0.97 dB at 40 GHz and out-of-band rejection of larger than 23 dB, while the filter with the interdigital coupled-lines realizes the suppressions in lower and upper-bands of, respectively, larger than 30 dB and 19 dB for the overall insertion loss of 2.1 dB at 40 GHz.

1. INTRODUCTION

In communication systems, bandpass filters are the key circuit blocks for preventing signal interference and unwanted signal rejection. Low-loss waveguide bandpass filters have long been used. However, they are bulky and expensive for applications in the millimeter-wave (mmW) bands due to critical tolerance requirements and difficulty to be

Received 24 November 2012, Accepted 21 December 2012, Scheduled 4 January 2013

* Corresponding author: Sai Wai Wong (eewsw@scut.edu.cn).

integrated with other circuits. Alternatively, microstrip-line circuits are popular due to their merits such as low cost, compact size and easy integration.

On the other hand, a bandpass filter with transmission zeros near the lower and upper cut-off frequencies is the most effective implementation of a bandpass filter with high selectivity. Numerous bandpass filters, adopting different approaches to produce transmission zeros at the lower and upper stopbands have been reported in [1–17]. A straightforward way to produce two transmission zeros is to use two shunt open-circuited stubs of different lengths [1–4]. Another method is to use the two-path approach [4–12]. The two-path microstrip-line bandpass filter consists of hairpin resonators with asymmetric tapped feed lines [4, 5]. These asymmetric tapped feeding lines were also used with a stepped impedance resonator in a bandpass filter [6–9]. Another example of the two-path approach was the signal interference technique used for the transversal filters [10–13]. This technique produces multiple transmission zeros at the lower and upper-stopbands. In addition, a feedback capacitor has been used in different types of coupled resonators to produce two transmission zeros [14–16]. Recently, an open-loop filter with mixed coupling was studied for its transmission zeros at the lower and upper stopbands [17] and dual-mode loop resonator also can achieve transmission zeros to improve out-of-band rejection[18, 19].

Moreover, parallel coupled-lines and interdigital coupled-lines are widely used in bandpass filter design to reject the lower and upper-stopbands due to their bandpass properties [20–28].

In this paper, a rotationally symmetric short-circuited stub-loaded structure is proposed in the design of a microstrip-line bandpass filter with two transmission zeros near the lower and upper cut-off frequency edges of operating mmW bands. Simple transmission line models are derived to study the performance of two-path filters with rotationally symmetrical structures. Then a rotationally symmetric filter prototype is fabricated in a single circuit layer using low temperature co-fired ceramic (LTCC) technology. After that, interdigital coupled-lines are integrated into the rotationally symmetric structure to sharpen the rejection skirt. Last, the proposed filter is also fabricated in a single layer using LTCC technology in the mmW frequency range. All the filters herein will be optimized using CST studio, an electromagnetic (EM) simulator.

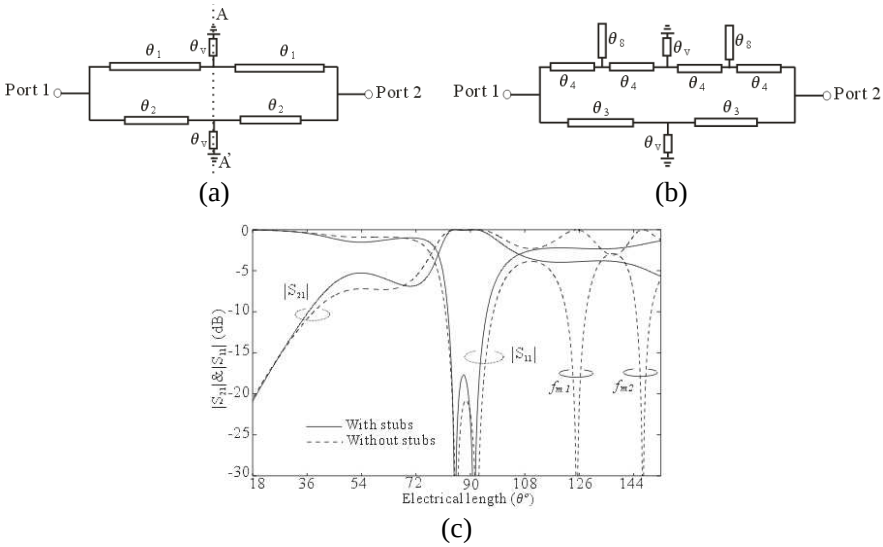

Figure 1. (a) Transmission line model of vertically symmetric filter. (b) Transmission line model of vertically symmetric filter with open-circuited stubs. (c) Calculated $|S_{21}|$ and $|S_{11}|$ of the two filter models.

2. CIRCUIT MODEL OF ROTATIONALLY SYMMETRICAL STRUCTURE BANDPASS FILTER

The initial filter design stems from a simple transmission line model as shown in Figure 1(a). The filter model is symmetrical about the center of the vertical plane (A-A' plane). The signal from the input port, Port 1 or 2 is divided into two portions when passing through this two-path filter. The divided signals are then merged at the output port, Port 2 or 1. The impedance of the two models Z is chosen as $70\,\Omega$, which can be easily implemented. The $|S_{21}|$ and $|S_{11}|$ are calculated from converting the resultant Y-matrix by adding the Y-matrix of upper and lower path. The $|S_{21}|$ and $|S_{11}|$ are plotted in Figure 1(c) (dotted lines: $\theta_1 = 205°$, $\theta_2 = 132°$, $\theta_v = 15°$). Since the equivalent electrical lengths for the upper and lower path are different, signal interference occurs when these two signals are combined at the output port [11]. This signal-interference technique is expected to generate the transmission zeros in the lower and upper stopbands, hence forming the stopbands as shown in the Figure 1(c) (dotted lines). However, this model suffers from unwanted resonance modes, at f_{m1} and f_{m2}. Figure 1(c) shows the calculated $|S_{21}|$ and $|S_{11}|$ of the Figure 1(b) (solid line: $\theta_3 = 140°$, $\theta_4 = 75°$, $\theta_8 = 50°$, $\theta_v = 15°$). It is found that

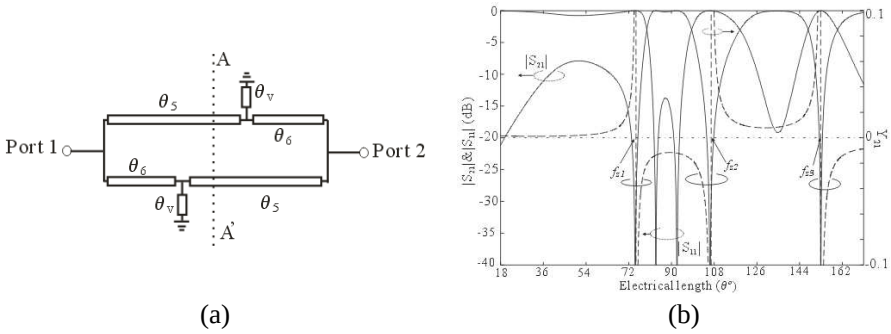

(a) (b)

Figure 2. (a) Transmission line model of rotationally symmetric filter. (b) Calculated $|S_{21}|$, $|S_{11}|$ and Y_{21} of the filter model.

the unwanted resonance modes f_{m1} and f_{m2} are removed, whereas the passband with better than 17 dB return loss remains unchanged. The two transmission line models as shown in Figure 1 attain good passbands at the electrical length of around 90°. The higher order modes f_{m1} and f_{m2} have been removed by adding the open-circuited stubs as shown in Figure 1(b). However, the rejection of the out-of-bands of these two filters is poor.

The two transmission line models as shown in Figure 1(a) and Figure 1(b) attain good passbands at the electrical length θ of around 90° as shown in Figure 1(c). The higher order modes f_{m1} and f_{m2} have been removed by adding the open-circuited stubs as shown in Figure 1(b). However, the rejection of the out-of-bands of these two filters is still poor. Thus, the transmission line model as shown in Figure 2(a) is proposed. Instead of using the vertically symmetrical structure as shown in the Figure 1, the two short-circuited stubs are offset from the center of vertical plane (plane A-A'). Thus, a rotationally symmetric structure is formed as shown in Figure 2(a). The $|S_{21}|$ and $|S_{11}|$ are plotted in Figure 2(b) (solid lines: $\theta_5 = 200°$, $\theta_6 = 140°$, $\theta_v = 15°$). The transmission zeros can be easily derived from the circuit model. The Y_{12} of this model is derived as

$$Y_{12} = \frac{2j}{Z\sin(\theta_5 + \theta_6) + Z^2 \sin\theta_5 \cos\theta_6/(Z_v \tan\theta_v)} \tag{1}$$

The results from (1) are also plotted in Figure 2(b) in a long dotted line. The transmission zeros are calculated using the intersection points of (1) and $Y_{12} = 0$ in the short dotted line. As observed from Figure 2(b), three transmission zeros at f_{z1}, f_{z2} and f_{z3} appear at the intersection points. Notably, the rejection skirt is dramatically sharpened with the zeros at f_{z1} and f_{z2}.

As shown in Figure 1(b), the open-circuited stubs can be used to remove the unwanted higher order modes. The same approach is applied in the design as shown in Figure 2 to suppress the unwanted passband ranged from $\theta = 126°$ to $144°$. Figure 3(b) plots the $|S_{21}|$ and $|S_{11}|$ results of the design which is shown in Figure 3(a) (solid lines: $\theta_6 = 146°$, $\theta_7 = 70°$, $\theta_8 = 50°$, $\theta_v = 15°$). For comparison purpose, the $|S_{21}|$ and $|S_{11}|$ of Figure 2(a) are also shown in Figure 3(b) (dotted lines). As observed from Figure 3(b), the unwanted passband ranging from $\theta = 126°$ to $144°$ is suppressed to below -11 dB. Whereas, the first two transmission zeros (at f_{z1}, f_{z2}) and the two poles in the passband remain almost unchanged. The third transmission zero at f_{z3} is shifted from $\theta = 153°$ to a higher band at $\theta = 162°$ in order to widen the upper-stopband. As a result, an enhanced in-band and out-of-band bandpass filter model is constructed using a rotationally symmetric structure.

3. CIRCUIT MODEL OF ROTATIONALLY SYMMETRICAL STRUCTURE BANDPASS FILTER WITH COUPLING EFFECTS

The aforementioned transmission line models are realized using microstrip-line circuits in this section. However, if the transmission

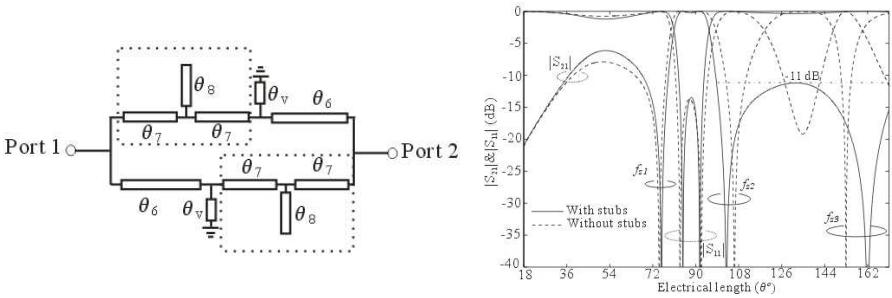

Figure 3. (a) Transmission line model of rotationally symmetric filter with open-circuited stubs. (b) Calculated $|S_{21}|$ and $|S_{11}|$ of two rotationally symmetric filter models with and without open-circuited stubs.

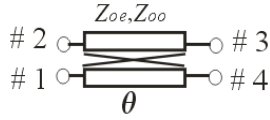

Figure 4. Transmission line model of coupled-line.

lines in the upper and lower sections are close to each other during circuit implementation, coupling effects should be taken into account using the coupled-line model as shown in Figure 4.

The Z-matrix elements of the transmission line are listed below [20]:

$$z_{11} = z_{22} = z_{33} = z_{44} = -j/2(z_{oe} + z_{oo})\cot(\theta) \tag{2a}$$
$$z_{12} = z_{21} = z_{34} = z_{43} = -j/2(z_{oe} - z_{oo})\cot(\theta) \tag{2b}$$
$$z_{13} = z_{31} = z_{24} = z_{42} = -j/2(z_{oe} - z_{oo})\csc(\theta) \tag{2c}$$
$$z_{14} = z_{41} = z_{23} = z_{32} = -j/2(z_{oe} + z_{oo})\csc(\theta) \tag{2d}$$

For instance, the model as shown in Figure 2(a) should be reconstructed as shown in Figure 5(a). The circuit can be divided into three parts namely $\mathcal{Z}^a$, $\mathcal{Z}^b$ and $\mathcal{Z}^a$.

The $\mathcal{Z}^a$ parts can be seen as a simple transmission lines and the $\mathcal{Z}^b$ part can be describe as two short-circuit stubs on a simple transmission lines, and the $\mathcal{Z}^b$-matrix of the structure in terms of coupled-line Z-matrix elements showed in Figure 5(a) is given below:

$$Z^b_{11} = Z^b_{33} = Z_{Ls}\frac{z_{11}(Z_{Ls} - z_{11}) + z_{13}^2}{Z_{Ls}^2 - z_{11}^2 + z_{13}^2}$$
$$Z^b_{12} = Z^b_{34} = Z_{Ls}\frac{z_{13}z_{14} - z_{11}z_{12} + z_{12}Z_{Ls}}{(Z_{Ls} - z_{11})^2 - z_{13}^2}$$
$$Z^b_{13} = Z^b_{31} = Z_{Ls}\frac{z_{13}(Z_{Ls} - z_{11}) + z_{11}z_{13}}{Z_{Ls}^2 - z_{11}^2 + z_{13}^2}$$
$$Z^b_{14} = Z^b_{32} = Z_{Ls}\frac{z_{12}z_{13} - z_{11}z_{14} + z_{14}Z_{Ls}}{(Z_{Ls} - z_{11})^2 - z_{13}^2}$$
$$Z^b_{21} = Z^b_{43} = Z_{Ls}\frac{z_{12}(Z_{Ls} - z_{11}) + z_{13}z_{14}}{Z_{Ls}^2 - z_{11}^2 + z_{13}^2}$$

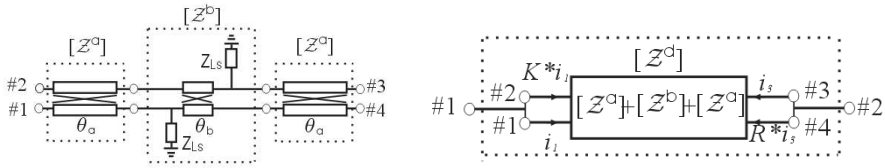

Figure 5. (a) Transmission line model of rotationally symmetric filter. (b) The equivalent network of the rotationally structure.

$$Z_{22}^b = Z_{44}^b = z_{22} + \frac{2z_{12}z_{13}z_{14} + (z_{12}^2 + z_{14}^2)(Z_{Ls} - z_{11})}{(Z_{Ls} - z_{11})^2 - z_{13}^2}$$

$$Z_{23}^b = Z_{41}^b = Z_{Ls}\frac{z_{14}(Z_{Ls} - z_{11}) + z_{12}z_{13}}{Z_{Ls}^2 - z_{11}^2 + z_{13}^2}$$

$$Z_{24}^b = Z_{42}^b = z_{24} + \frac{z_{13}(z_{12}^2 + z_{14}^2) + 2z_{12}z_{14}(Z_{Ls} - z_{11})}{(Z_{Ls} - z_{11})^2 - z_{13}^2}$$

where, the Z_{Ls} is modeling the loading effects of vias.

Figure 5(b) showed the equivalent network of the rotationally structure, and $\mathcal{Z}^d$ can be easily obtain by simple matrix addition that is $\mathcal{Z}^d = \mathcal{Z}^a(\theta_a) + \mathcal{Z}^b(\theta_b) + \mathcal{Z}^a(\theta_a)$.

By introducing two current ratios namely K and R to make the four ports network to two ports network, and the two port network Z-matrix of the Figure 5(b) obtains below by introducing the K and R:

$$Z_{11} = \frac{Z_{11}^d + kZ_{11}^d}{1+k} + \frac{Z_{13}^d - Z_{14}^d}{1+k}\frac{Z_{11}^d + kZ_{12}^d - Z_{21}^d - Z_{22}^d}{Z_{23}^d - Z_{24}^d - Z_{13}^d + Z_{14}^d}$$

$$Z_{12} = \frac{Z_{12}^d - Z_{11}^d}{1+R}\frac{Z_{13}^d + Z_{23}^d + R\left(Z_{14}^d + Z_{24}^d\right)}{Z_{11}^d - Z_{12}^d - Z_{21}^d + Z_{22}^d}$$

$$Z_{21} = \frac{Z_{31}^d + kZ_{32}^d}{1+k} + \frac{Z_{33}^d - Z_{34}^d}{1+k}\frac{Z_{11}^d + kZ_{12}^d - Z_{21}^d - kZ_{22}^d}{Z_{23}^d - Z_{24}^d - Z_{13}^d + Z_{14}^d}$$

$$Z_{22} = \frac{Z_{32}^d - Z_{31}^d}{1+R}\frac{Z_{13}^d + Z_{23}^d + R\left(Z_{14}^d + Z_{24}^d\right)}{Z_{11}^d - Z_{12}^d - Z_{21}^d + Z_{22}^d} + \frac{Z_{33}^d + RZ_{34}^d}{1+R}$$

The transmission line model of the filter with the open-circuited stubs which shown in Figure 3(a) should be re-constructed as shown in Figure 6, and it can be divided into three parts namely $\mathcal{Z}^{a'}$, $\mathcal{Z}^{b'}$

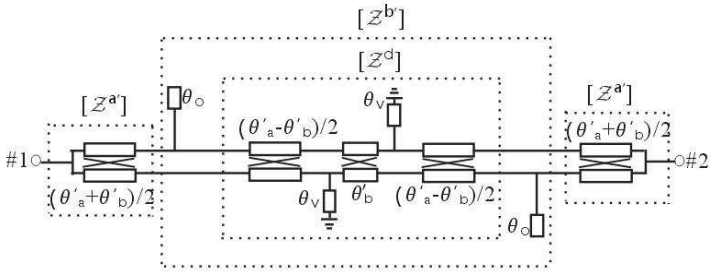

Figure 6. Circuit model with coupling effect with open stub loaded structure.

and $\mathcal{Z}^{a'}$ as shown in Figure 6. The $\mathcal{Z}^{a'}$ parts can be seen as a simple coupled lines and the $\mathcal{Z}^{b'}$ part can be describe as two open-circuit stub loaded on $\mathcal{Z}^{d}$ circuit in Figure 5(b).

Thus, $\mathcal{Z}^{b'}$ can be similar derived from the $\mathcal{Z}^{d}$-matrix. The obtained $\mathcal{Z}^{b'}$-matrix is showed below:

$$Z_{11}^{b'} = Z_{33}^{b'} = Z_{Lo}\frac{Z_{11}^{d}\left(Z_{Lo} - Z_{11}^{d}\right) + \left(Z_{13}^{d}\right)^{2}}{Z_{Lo} - \left(Z_{11}^{d}\right)^{2} + \left(Z_{13}^{d}\right)^{2}}$$

$$Z_{12}^{b'} = Z_{34}^{b'} = Z_{Lo}\frac{Z_{13}^{d}Z_{14}^{d} - Z_{11}^{d}Z_{12}^{d} + Z_{12}^{d}Z_{Lo}}{\left(Z_{Lo} - Z_{11}^{d}\right)^{2} + \left(Z_{13}^{d}\right)^{2}}$$

$$Z_{13}^{b'} = Z_{31}^{b'} = Z_{Lo}\frac{Z_{13}^{d}\left(Z_{Lo} - Z_{11}^{d}\right) + Z_{11}^{d}Z_{13}^{d}}{\left(Z_{Lo} - Z_{11}^{d}\right)^{2} + \left(Z_{13}^{d}\right)^{2}}$$

$$Z_{14}^{b'} = Z_{32}^{b'} = Z_{Lo}\frac{Z_{12}^{d}Z_{13}^{d} - Z_{11}^{d}Z_{14}^{d} + Z_{14}^{d}Z_{Lo}}{\left(Z_{Lo} - Z_{11}^{d}\right)^{2} - (Z_{13}^{d})^{2}}$$

$$Z_{21}^{b'} = Z_{43}^{b'} = Z_{Lo}\frac{Z_{12}^{d}\left(Z_{Lo} - Z_{11}^{d}\right) + Z_{13}^{d}Z_{14}^{d}}{\left(Z_{Lo}\right)^{2} - \left(Z_{11}^{d}\right)^{2} + \left(Z_{13}^{d}\right)^{2}}$$

$$Z_{22}^{b'} = Z_{44}^{b'} = Z_{22}^{d} + \frac{2Z_{12}^{d}Z_{13}^{d}Z_{14}^{d} + \left[\left(Z_{12}^{d}\right)^{2} + \left(Z_{14}^{d}\right)^{2}\right]\left(Z_{Lo} - Z_{11}^{d}\right)}{\left(Z_{Lo} - Z_{11}^{d}\right)^{2} - \left(Z_{13}^{d}\right)^{2}}$$

$$Z_{23}^{b'} = Z_{41}^{b'} = Z_{Lo}\frac{Z_{14}^{d}\left(Z_{Lo} - Z_{11}^{d}\right) + Z_{12}^{d}Z_{13}^{d}}{\left(Z_{Lo}\right)^{2} - \left(Z_{11}^{d}\right)^{2} + \left(Z_{13}^{d}\right)^{2}}$$

$$Z_{24}^{b'} = Z_{42}^{b'} = Z_{24}^{d} + \frac{2Z_{12}^{d}Z_{14}^{d}\left(Z_{Lo} - Z_{11}^{d}\right) + Z_{13}^{d}\left[\left(Z_{12}^{d}\right)^{2} + \left(Z_{14}^{d}\right)^{2}\right]}{\left(Z_{Lo} - Z_{11}^{d}\right)^{2} - \left(Z_{13}^{d}\right)^{2}}$$

where, the Z_{Lo} is modeling the loading effects of open-circuited stub.

4. IMPLEMENTATION OF A ROTATIONALLY SYMMETRIC STRUCTURE BANDPASS FILTER IN MICROSTRIP LINE

The aforementioned transmission line models are realized using microstrip-line circuits in this section. Two transmission zeros can be obtained by the proposed rotationally structure in previous discussion. Here, we give a comparison between symmetric structure and rotationally symmetric structure which showed in Figure 7.

Then, two filters in the form of microstrip-lines are fabricated at 40 GHz. One is the vertically symmetric structure as shown in

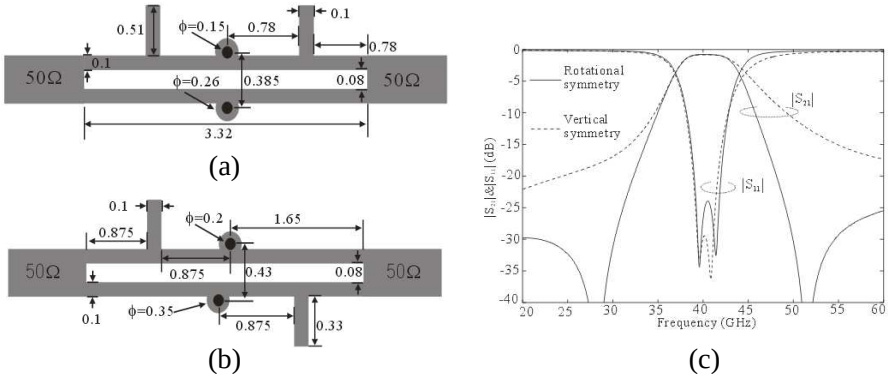

Figure 7. (a) Circuit layout and marked dimensions of vertically symmetric filter (in mm). (b) Circuit layout and marked dimensions of rotationally symmetric filter (in mm). (c) Simulated $|S_{21}|$ and $|S_{11}|$ of two filters.

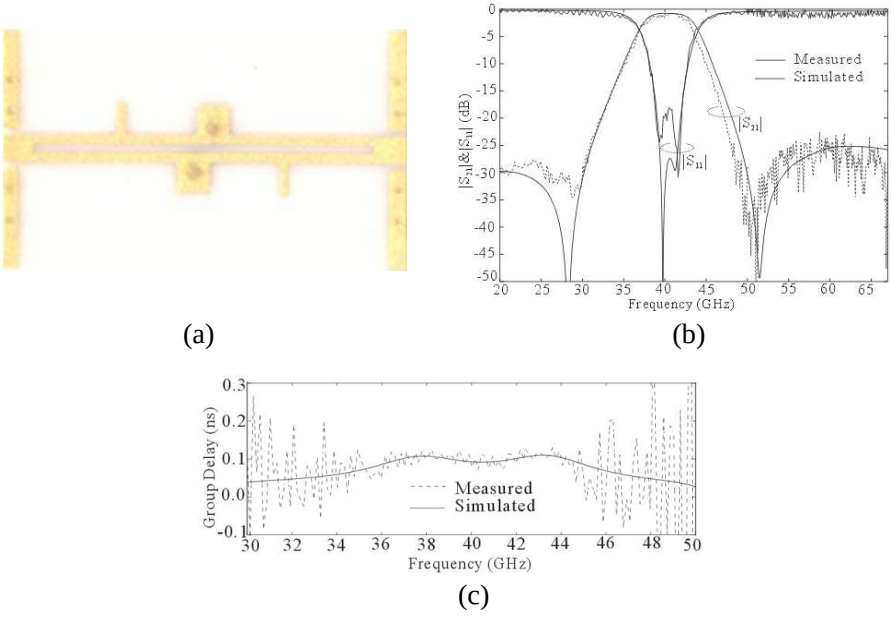

Figure 8. Predicted and measured frequency responses of the proposed rotationally symmetric bandpass filter. (a) Top-view photograph. (b) $|S_{21}|$ and $|S_{11}|$. (c) Group delay.

Figure 1(b). The other one is the rotationally symmetric structure as shown in Figure 3(a). Figures 7(a) and 7(b) depict the circuit layout with all the dimensions of the filter models in Figure 1(b) and Figure 3(a), respectively. It is noteworthy that the short-circuited stubs θ_v in the transmission line models are implemented as through vias, grounding the upper and lower microstrip-line sections. Figure 7(c) shows the simulated $|S_{21}|$ and $|S_{11}|$ of the designs shown in Figures 7(a) and 7(b). Though both filters have almost the same passband performance, the rotationally symmetric structure exhibits sharper rejection skirt than the vertically symmetric structure because the two transmission zeros generated in the rotationally symmetric filter are very close to the lower and upper cut-off edges of the passband. The simulation shows that the rotationally symmetric filter has the 3-dB bandwidth of 16%, 0.66-dB insertion loss at 40 GHz, and out-of-band rejection of larger than 25 dB.

The rotationally symmetric filter in Figure 7(b) was fabricated using LTCC technology. The substrate used herein has a dielectric constant of 5.9, a substrate thickness of 0.193 mm and a loss tangent of 0.002. Figure 8(a) shows the top-view photograph of the filter with two ground-signal-ground (GSG) transitions for probe station measurement. The measured and simulated $|S_{21}|$ and $|S_{11}|$ results are plotted in Figure 8(b). The measured insertion loss at the center frequency of 40 GHz is 0.97 dB, including the GSG transitions loss. The measured lower and upper stopbands rejections are larger than 23 dB. Figure 8(c) shows the measured and simulated group delay with the small variation of less than 0.03 ns across the passband.

5. ROTATIONALLY SYMMETRIC STRUCTURE BANDPASS FILTER USING INTERDIGITAL COUPLED-LINES

The interdigital coupled-lines are proposed to improve the out-of-band performance of the proposed rotationally symmetric microstrip-line bandpass filter. Figure 9(a) illustrates the layout with the detailed dimensions of the proposed filter. The rotationally symmetric structure is divided into the upper and lower resonators. The input power is coupled to the two resonators through the two sections of one-quarter guided wavelength ($\lambda_g/4$, λ_g at 40 GHz) interdigital coupled-lines sections.

Figure 9(b) depicts the transmission line model of the filter. The modeling of the interdigital coupled-lines involves c-mode and π-mode due to the asymmetrical coupling [21, 22]. As known, it is difficult to convert both the c-mode and π-mode to physical dimensions in

filter design. Thus, both the c-mode and π-mode are simplified into the even-mode and odd-mode [29]. The simulated $|S_{21}|$ and $|S_{11}|$ are shown in Figure 9(c), compared with that of the design as shown in Figure 8(b). Obviously, the filter with interdigital coupled-lines (solid lines) has achieved a sharper roll-off rejection skirt than the filter shown in Figure 8(b) (dotted line) because of the two transmission zeros of the interdigital coupled-lines filter closer to the cut-off edges of the passband. Moreover, the upper-stopband is dramatically improved even beyond 100 GHz. The unwanted passband ranging from 78 to 95 GHz is suppressed from -5 dB to below -30 dB as shown in the Figure 9(c) at a price of a slightly higher passband insertion loss. The simulated insertion loss is 1.07 dB at the center frequency of 40 GHz of the passband. The 3-dB fractional bandwidth of 40 GHz is 20%.

Figure 10(a) depicts the layout and dimensions of the interdigital coupled-lines filter with additional resonators. Based on the structure as shown in Figure 9(a), four sections of one half guided wavelength ($\lambda_g/2$) resonators are added to the rotationally symmetric resonator. This is modeled as the two sections of $\lambda_g/2$ parallel coupled-lines as shown in Figure 10(b). Figure 10(c) shows the simulated $|S_{21}|$ using strong ($d = 0.85$ mm) and weak coupling ($d = 0.25$ mm) of the design as shown in Figure 10(a). $|S_{21}|$ for the weak coupling scheme shows that the passband is constructed by four resonance modes at f_{m1}, f_{m2}, f_{m3} and f_{m4}. $|S_{21}|$ for the strong coupling scheme (solid line) shows that the improved passband and out-of-band performances of this proposed filter. The out-of-band performances are also improved compared with that of the filter as depicted in Figure 9(a). In particular, the lower

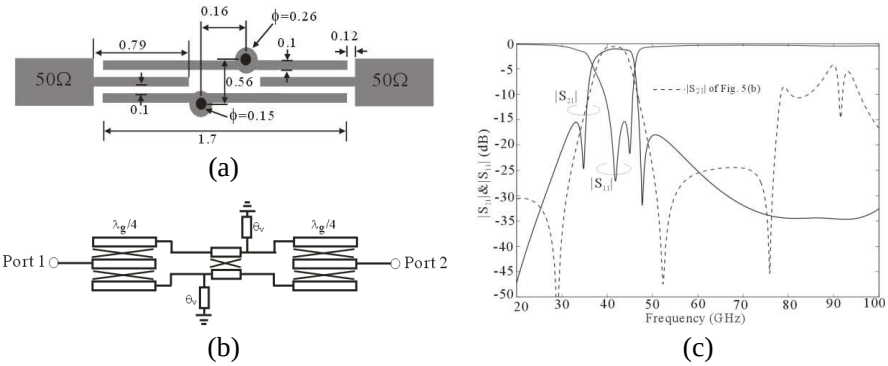

Figure 9. (a) Circuit layout and marked dimensions (in mm). (b) Transmission line model. (c) $|S_{21}|$ and $|S_{11}|$ of the interdigital coupled-lines bandpass filter.

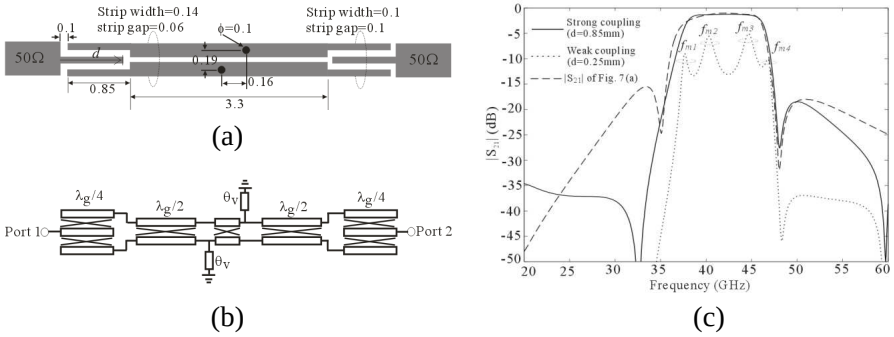

Figure 10. (a) Circuit layout and marked dimensions (in mm). (b) Transmission line model. (c) $|S_{21}|$ and $|S_{11}|$ of the interdigital coupled-lines bandpass filter with additional resonators.

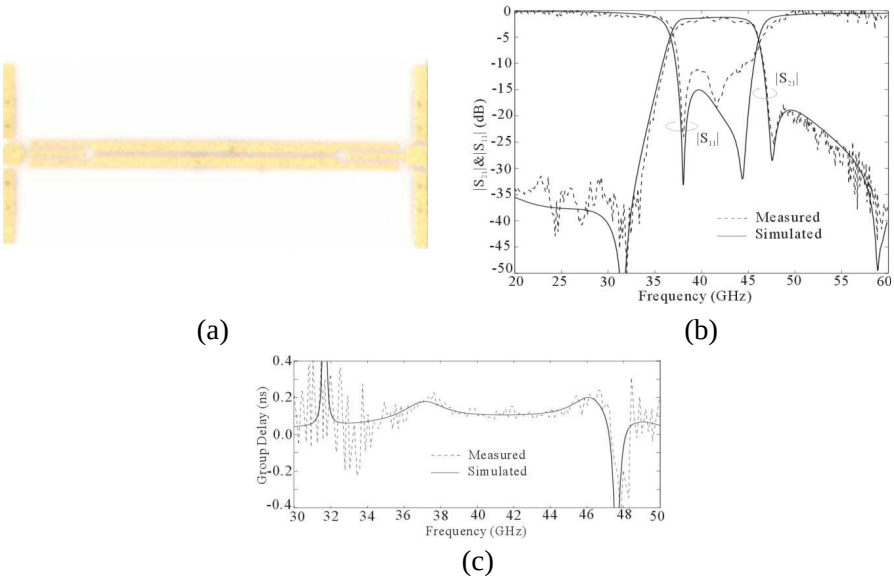

Figure 11. Predicted and measured frequency responses of the proposed interdigital coupled-lines bandpass filter: (a) Top-view photograph. (b) $|S_{21}|$ and $|S_{11}|$. (c) Group delay.

stopband is suppressed from −16 dB to below −30 dB as shown in Figure 10(c). The simulated insertion loss is 1.13 dB at 40 GHz and the 3-dB fractional bandwidth range from 37.5 to 46.5 GHz is 21%.

6. EXPERIMENTAL RESULTS

To verify the design, a 40-GHz microstrip-line bandpass filter with GSG to microstrip-line transitions was fabricated on a single layer LTCC with the same substrate as one used above. The top-view photograph of the filter circuit is shown in Figure 11(a). Besides the GSG to microstrip-line transitions, the filter dimensions follow those indicated in the Figure 10(a). Figures 11(b) and 11(c) show the comparison between the predicted and measured frequency responses of $|S_{21}|$ and $|S_{11}|$ as well as group delay (two transitions included). The agreement between the simulation and measurement results is acceptable at such high frequencies. Thereby the actual realization of the preferred 40-GHz passband was well confirmed in measurement. The measured and simulated insertion loss with transitions is 2.1 dB and 1.4 dB at 40 GHz of the passband, respectively. The 3-dB fractional bandwidth ranged from 37.6 to 46.5 GHz is 21%. Moreover, the measured group delay varies between 0.1–0.2 ns within the passband showing a good linearity.

7. CONCLUSION

In this work, the rotationally symmetric microstrip-line bandpass filters have been proposed and studied as well as designed at 40 GHz bands. The transmission line models of vertically symmetric structure and rotationally symmetric structure have been discussed and used to examine the in-band and out-of-band performances of the bandpass filters. The study has showed that the rotationally symmetric structures have achieved better rejection with the transmission zeros close to the cut-off frequencies of the passband. The measured results of one rotationally symmetric filter have shown the 0.97-dB insertion loss at 40 GHz. The lower and upper stopbands rejections are larger than 23 dB. Then, the rotationally symmetric structure has been integrated with interdigital coupled-lines to further sharpen the rejection skirt and widen the stopband beyond 100 GHz. In addition, four half-guided-wavelength sections of microstrip-lines have been attached to the rotationally symmetric resonator to further improve the out-of-band performances. Last, a microstrip-line bandpass filter prototype with the GSG to microstrip-line transitions operating at 40 GHz bands has been fabricated to experimentally verify the design. The measured results of the filter have showed that the suppressions in the lower and upper-bands are, respectively, larger than 30 dB and 19 dB, and the measured insertion loss is 2.1 dB at 40 GHz.

ACKNOWLEDGMENT

This work is supported by the National Natural Science Foundation of China (61101017) and the State Key Laboratory of Millimeter Waves (K201327), Southeast of University.

REFERENCES

1. Zhu, L. and W. Menzel, "Compact microstrip bandpass filter with two transmission zeros using a stub-trapped half-wavelength line resonator," *IEEE Microwave Wireless Compon. Lett.*, Vol. 13, No. 1, 16–18, Jan. 2003.
2. Gan, H., D. Lou, and D. Yang, "Compact microstrip bandpass filter with sharp transition bands," *IEEE Microwave Wireless Compon. Lett.*, Vol. 16, No. 3, 107–109, Mar. 2006.
3. Choi, S.-U., M.-S. Chung, and S.-W. Yun, "Hairpin tunable bandpass filter with improved selectivity and tunability," *Asia-Pacific Conf. Proceedings*, Vol. 10, 1–4, Dec. 2007.
4. Hsieh, L.-H. and K. Chang, "Tunable microstrip bandpass filters with two transmission zeros," *IEEE Trans. Microwave Theory Tech.*, Vol. 51, No. 2, 520–525, Feb. 2003.
5. Yang, M. H., J. Xu, Q. Zhao, L. Peng, and G. P. Li, "Compact broad-stopband lowpass filter using SIRs-loaded circular hairpin resonators," *Progress In Electromagnetics Research*, Vol. 102, 95–106, 2010.
6. Kuo, J.-T., C.-L. Hsu, and E. Shih, "Compact planar quasic-elliptic function filter with inline stepped-impedance resonators," *IEEE Trans. Microwave Theory Tech.*, Vol. 55, No. 8, 1747–1755, Aug. 2007.
7. Djaiz, A. and T. A. Denidni, "A new compact microstrip two-layer bandpass filter using aperture-coupled SIR-hairpin resonators with transmission zeros," *IEEE Trans. Microwave Theory Tech.*, Vol. 54, No. 5, 1929–1936, May 2006.
8. Zhang, J., J.-Z. Gu, B. Cui, and X. W. Sun, "Compact and harmonic suppression open-loop resonator bandpass filter with tri-section SIR," *Progress In Electromagnetics Research*, Vol. 69, 93–100, 2007.
9. Ma, D.-C., Z.-Y. Xiao, L.-L. Xiang, X.-H. Wu, C.-Y. Huang, and X. Kou, "Compact dual-band bandpass filter using folded SIR with two stubs for WLAN," *Progress In Electromagnetics Research*, Vol. 117, 357–364, 2011.
10. Deng, P.-H., Y.-S. Lin, C.-H. Wang, and C. H. Chen, "Compact

microstrip bandpass filters with good selectivity and stopband rejection," *IEEE Trans. Microwave Theory Tech.*, Vol. 54, No. 2, 533–539, Feb. 2006.

11. Gomez-Garcia, R. and J. I. Alonso, "Design of sharp-rejection and low-loss wide-band planar filters using signal-interference techniques," *IEEE Microwave Wireless Compon. Lett.*, Vol. 15, No. 8, 530–532, Aug. 2005.
12. Zhu, Y.-Z., Y.-J. Xie, and H. Feng, "Novel microstrip bandpass filters with transmission zeros," *Progress In Electromagnetics Research*, Vol. 77, 29–41, 2007.
13. Xiao, J.-K. and Q.-X. Chu, "Novel microstrip triangular resonator bandpass filter with transmission zeros and wide bands suing fractal-shaped defection," *Progress In Electromagnetics Research*, Vol. 77, 343–356, 2007.
14. Yeung, L. K. and K.-L. Wu, "A compact second-order LTCC bandpass filter with two finite transmission zeros," *IEEE Trans. Microwave Theory Tech.*, Vol. 51, No. 2, 337–341, Feb. 2003.
15. Wu, C.-H., Y.-S. Lin, C.-H. Wang, and C. H. Chen, "Novel microstrip coupled-line bandpass filters with shortened coupled sections for stopband extension," *IEEE Trans. Microwave Theory Tech.*, Vol. 54, No. 2, 540–546, Feb. 2006.
16. Martinez-Mendoza, M., J. S. Gomez-Diaz, D. Canete-Rebenaque, J. L. Gomez-Tornero, and A. Alvarez-Melcon, "Design of bandpass transversal filters employing a novel hybrid structure," *IEEE Trans. Microwave Theory Tech.*, Vol. 55, Vol. 12, 2670–2678, Dec. 2007.
17. Chu, Q.-X. and H. Wang, "A compact open-loop filter with mixed electric and magnetic coupling," *IEEE Trans. Microwave Theory Tech.,* Vol. 56, No. 2, 431–439, Feb. 2008.
18. Chen, Z.-X., X.-W. Dai, and C.-H. Liang, "Novel dual-mode dual-band bandpass filter using double square-loop structure," *Progress In Electromagnetics Research*, Vol. 77, 409–416, 2007.
19. Wu, G.-L., W. Mu, X.-W. Dai, and Y.-C. Jiao, "Design of novel dual-band bandpass filter with microstrip meander-loop resonator and CSRR DGS," *Progress In Electromagnetics Research*, Vol. 78, 17–24, 2008.
20. Zysman, G. I. and A. K. Johnson, "Coupled transmission line networks in an inhomogeneous dielectric medium," *IEEE Trans. Microwave Theory Tech.*, Vol. 17, No. 10, 753–759, Oct. 1969.
21. Schwindt, R. and C. Nguyen, "Spectral domain analysis of three symmetric coupled lines and application to a new bandpass filter,"

IEEE Trans. Microwave Theory Tech., Vol. 42, No. 7, 1183–1189, Jul. 1994.

22. Tripathi, V. K., "On the analysis of symmetrical three-line microstrip circuits," *IEEE Trans. Microwave Theory Tech.*, Vol. 25, No. 9, 726–729, Sep. 1977.
23. Wong, S. W. and L. Zhu, "EBG-embedded multiple-mode resonator for UWB bandpass filter with improved upper-stopband performance," *IEEE Microwave Wireless Compon. Lett.*, Vol. 17, No. 6, 421–423, Jun. 2007.
24. Yamamoto, S., T. Azakami, and K. Itakura, "Coupled strip transmission line with three center conductors," *IEEE Trans. Microwave Theory Tech.*, Vol. 14, No. 10, 446–461, Oct. 1966.
25. Wenzel, R. J., "Exact theory of interdigital band-pass filters and related coupled structures," *IEEE Trans. Microwave Theory Tech.,* Vol. 5, No. 10, 559–575, Nov. 1969.
26. Tripathi, V. K., "The scattering parameters and directional coupler analysis of characteristically terminated three-line structures in an inhomogeneous medium," *IEEE Trans. Microwave Theory Tech.,* Vol. 29, No. 1, 22–26, Jan. 1981.
27. Ye, C. S., "Design of the compact parallel-coupled lines wideband bandpass filters using image parameter method," *Progress In Electromagnetics Research*, Vol. 100, 153–173, 2010.
28. Cui, D., Y. Liu, Y. Wu, S. Li, and C. Yu, "A compact bandstop filter based on two meandered parallel-coupled lines," *Progress In Electromagnetics Research*, Vol. 121, 271–279, 2011.
29. Hong, J. S. and M. J. Lancaster,*Microstrip Filters for RF/Microwave Applications,* Wiley, New York, 2001.